

# 1 A constant Chinese Loess Plateau dust source since the 2 Late Miocene

3 **Anna Bird<sup>1,2</sup>, Ian Millar<sup>3</sup>, Tanja Rodenburg<sup>2</sup>, Thomas Stevens<sup>2,4</sup>, Martin Rittner<sup>5</sup>, Pieter**  
4 **Vermeesch<sup>5</sup>, Huayu Lu<sup>6</sup>**

5 <sup>1</sup>*School of Environment Sciences, University of Hull, Hull, HU6 7RX, UK. [a.bird@hull.ac.uk](mailto:a.bird@hull.ac.uk)*

6 <sup>2</sup>*Department of Geography, Royal Holloway University of London, Egham, Surrey, TW20 0EX,*  
7 *UK*

8 <sup>3</sup>*NERC Isotope Geosciences Laboratory, British Geological Survey, Keyworth, UK*

9 <sup>4</sup>*Department of Earth Sciences, Uppsala University, Geocentrum, Villav. 16, 752 36 Uppsala,*  
10 *Sweden*

11 <sup>5</sup>*Department of Earth Sciences, University College London, London, WC1E 6BT, UK*

12 <sup>6</sup>*School of Geographic and Oceanographic Sciences, Nanjing University, Nanjing 210093,*  
13 *China*

14 The Pliocene-Pleistocene boundary marks a major change in global climate and East Asian  
15 monsoon dynamic. However, the role of the global atmospheric dust-cycle over this time is  
16 unclear; in particular the degree to which changes in the dust cycle influenced climate  
17 change, were driven by climate change, and how these processes interacted. Chinese loess  
18 records past dust-cycle history and the influences of aridification and monsoon circulation  
19 over the last 40 Ma. Previous work on the Chinese Loess Plateau argue over whether  
20 changes in dust source occur at the Pliocene-Pleistocene boundary, or at 1.2 Ma, despite  
21 these intervals marking major shifts in monsoon dynamics (Ding et al., 2000; Lu, 2015). We  
22 present Sr, Nd and Hf isotope data from multiple sites and show that dust source largely  
23 remains unchanged across these boundaries. Shifts in geochemistry are due to changes in  
24 grain-size and weathering. While the transport pathway (river, deserts, direct aeolian) is  
25 unclear, these tracer isotopes show that dust was dominantly sourced from the Northern  
26 Tibetan Plateau, with some input from the local bedrock. This shows that a major  
27 established and constant dust source on the Tibetan Plateau has been active and unchanged  
28 since late Miocene, despite dramatically changing climate conditions. Changes in loess  
29 accumulation are a function of climate change in Tibetan Plateau source regions rather than  
30 effects from increased aridification over the Pliocene-Pleistocene boundary.

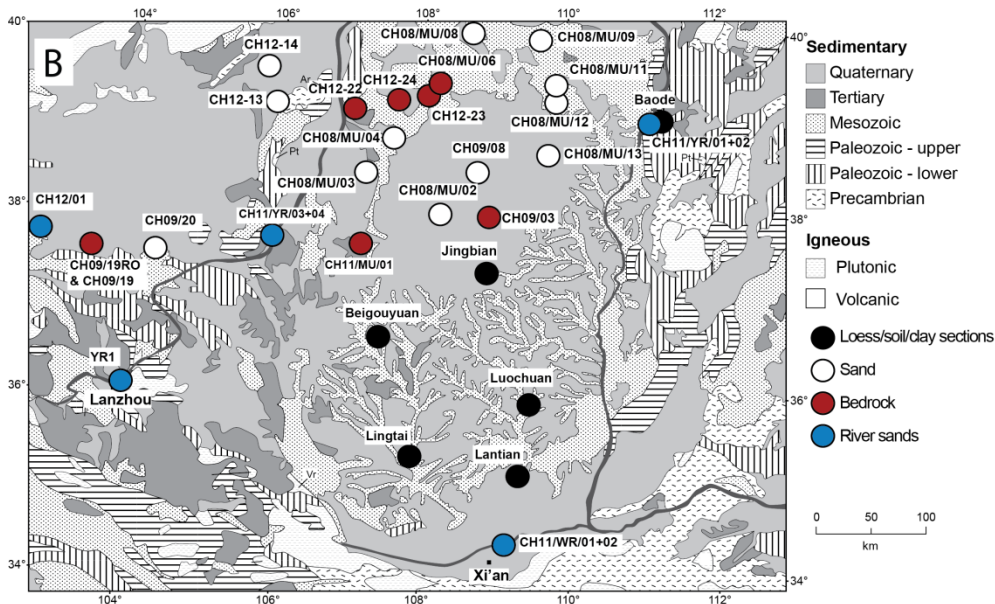
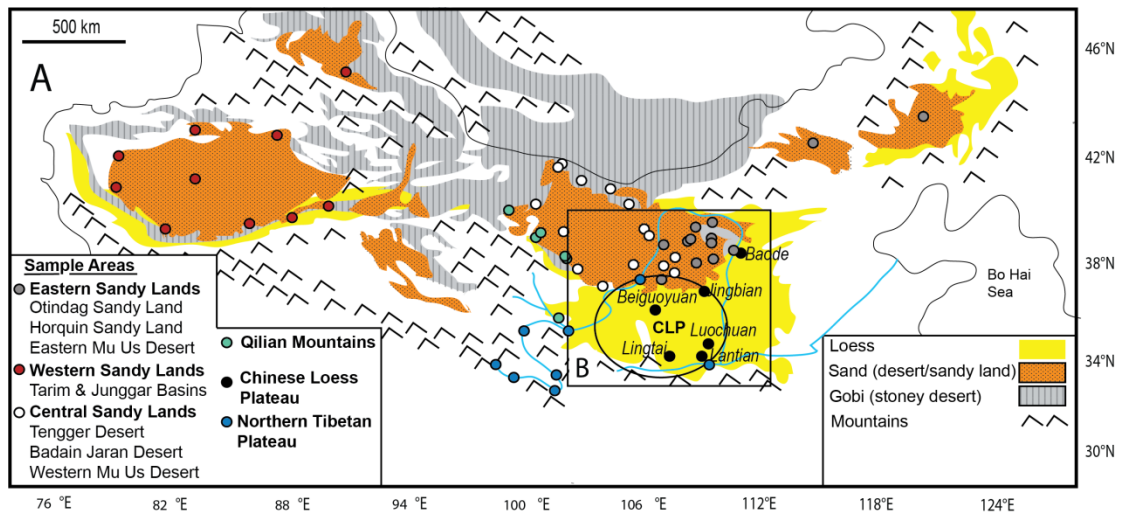
## 31 1 INTRODUCTION

32 Atmospheric dust dynamics play a central but poorly understood role in climate change,  
33 with past source activity identified as a key focus for future research (Merkel et al., 2014).  
34 Despite the significance for understanding Cenozoic global climate change, little is known  
35 about the evolution of the dust cycle during the major global climate reorganizations of the  
36 Pliocene and Quaternary. Wind-blown dust deposits on the Chinese Loess Plateau are  
37 recognized as one of the most valuable terrestrial climate archives available, spanning at  
38 least the last 25 Ma, making the sequence the longest and most continuous dust archive on  
39 the planet (Guo et al., 2002; Licht et al., 2016; Lu et al., 2010). The Loess Plateau is located in  
40 north-central China, and contains a near unique, detailed record of dust dynamics across the  
41 Pliocene and Quaternary. At 2.5 Ma a marked change is seen from Pliocene 'Red Clay'  
42 deposits to Quaternary soils and loess (Ding et al., 2000; Porter et al., 2001). The deposition  
43 and diagenesis of these sediments is intimately tied to climate, and the sources of Loess  
44 Plateau dust have been hypothesized to be a major controlling factor in glacial-interglacial  
45 climate changes in the Quaternary (Watson et al., 2000). What remains unclear is whether  
46 the shifts in climate and the nature of wind-blown dust across the Neogene and Quaternary  
47 are tied to shifts in dust source. This represents a major gap in understanding of how dust  
48 influences and responds to global and regional climate change.

49 Investigations into loess sources have used a variety of techniques including whole rock Nd  
50 and Sr isotopes, major and trace element chemistry, magnetic susceptibility, zircon U-Pb,  
51 and heavy mineral analysis. Each of these methods provides slightly different information  
52 about dust sources. For example, using whole rock Nd and Sr isotopes or major/trace  
53 elements to establish provenance has the advantage of allowing investigation of all grain-  
54 sizes and the disadvantage of averaging out potentially distinct sediment source signatures  
55 (e.g. Ding et al. 2002; Gallet et al. 1996). To tackle this issue, recent studies have used zircon  
56 U-Pb (Bird et al., 2015; Che and Li, 2013; Licht et al., 2016; Nie et al., 2015; Pullen et al.,  
57 2011; Stevens et al., 2013; Stevens and Lu, 2010; Xiao et al., 2012; Zhang et al., 2018, 2016).  
58 Most of these single-grain studies suggest that the northern Tibetan Plateau is the dominant  
59 source of the loess with input from the North China Craton (Bird et al., 2015; Che and Li,  
60 2013; Nie et al., 2015; Zhang et al., 2018, 2016). A problem with this approach is that zircons  
61 are predominantly derived from granitoids, inevitably biasing the dataset towards these  
62 sources. Furthermore, only the coarser (often  $>40\mu\text{m}$ ) zircons are analysed due to analytical  
63 limitations and this can introduce a size bias to data (e.g. Bird et al. 2015). Finally, as zircon is

64 an extremely robust mineral it can survive many cycles of sediment recycling and may not  
65 always provide insight into the most recent sediment transport phase.

66 Previous single grain and whole rock studies are unclear about the nature of dust source  
67 change through time. This is both true for whether variation in sources can be related to  
68 glacial/interglacial cycles (Jahn et al., 2001; Pullen et al., 2011; Sun et al., 2008) and for  
69 longer term source shifts. Changes in loess source have been reported at 1.2 Ma (Chen and  
70 Li, 2013; Sun, 2005), and 2.5 Ma (Chen et al., 2007; Nie et al., 2014; Sun and Zhu, 2010).  
71 These source changes are seen in  $^{87}\text{Sr}/^{86}\text{Sr}$  data, in some cases in  $^{143}\text{Nd}/^{144}\text{Nd}$  (e.g. Sun 2005;  
72 Chen & Li 2013) and in one case Pb isotopes (Sun and Zhu, 2010). In addition to these  
73 geochemical datasets the sequence on the Loess Plateau changes from loess/soil to Red Clay  
74 around the Pliocene-Pleistocene boundary at c. 2.5 Ma (e.g. Sun 2005). These studies  
75 suggest that there is a change in source or type of material delivered to the Plateau at this  
76 time. Other work suggests that the source was constant from 7 to 1.2 Ma when there was a  
77 decrease in the amount of material transported from the Qilian Mountains and a shift in  
78 palaeosol frequency (Chen and Li, 2013). However these potential variations in source are  
79 not seen in other studies using  $^{143}\text{Nd}/^{144}\text{Nd}$  (Gallet et al. 1996; Wang et al. 2007),  $^{176}\text{Hf}/^{177}\text{Hf}$   
80 (Chauvel et al., 2014) or some single grain zircon U-Pb studies (Bird et al., 2015). Thus, at  
81 present there is a major disagreement about a fundamental aspect of Cenozoic dust and  
82 climate evolution. Here we present new data from 134 samples (for full sample details see  
83 Supplementary Data Table 1) obtained from the Chinese Loess Plateau and potential source  
84 areas (see Fig. 1), along with published data, which demonstrate that dust sources show no  
85 systematic change from Miocene to Holocene times. This demonstrates that the sources of  
86 the majority of the Loess Plateau sediments show no systematic change, although proxies  
87 for individual components (e.g. zircon U-Pb) of loess do show variability, though there is  
88 disagreement on how systematic this variability is.



89

90 Figure 1, Samples and study area. A- showing the location of desert and river samples and the major Late  
 91 Cenozoic desert and loess deposits for samples within this study. B - Showing the location of samples from around  
 92 the Chinese Loess Plateau and Mu Us Desert, with sample numbers (for more details on samples see  
 93 Supplementary Data Table 1. Abbreviations are CLP - Chinese Loess Plateau; SR - Shui River; UB - Ulan Buh Sandy  
 94 Land; WR - Wey River. (Bird et al., 2015; Stevens et al., 2013).

## 95 2 METHODS

96 Nd, Sr and Hf analyses were undertaken at NIGL, Keyworth, UK on a single dissolution. The  
 97 whole rock powders were leached using 5 ml of 10 % acetic acid for 30 minutes at 60°C to  
 98 remove carbonate then washed in Milli-Q water and dried. Mixed  $^{149}\text{Sm}$ - $^{150}\text{Nd}$ ,  $^{176}\text{Lu}$ - $^{180}\text{Hf}$   
 99 and single  $^{84}\text{Sr}$  and  $^{87}\text{Rb}$  isotope tracers were then weighed and added and the samples were  
 100 digested by standard HF/ $\text{HNO}_3$  dissolution. Early samples were not mixed with the  $^{176}\text{Lu}$ - $^{180}\text{Hf}$   
 101 spike; these samples have no Hf concentration data. Hf, Nd and Sr were separated using  
 102 standard ion-exchange procedures.

103 Nd and Sr were analysed in a Thermo Scientific Triton mass spectrometer in multi-dynamic  
104 mode. Nd data were normalized to  $^{146}\text{Nd}/^{144}\text{Nd} = 0.7219$  and Sr data were normalized to  
105  $^{86}\text{Sr}/^{88}\text{Sr} = 0.1194$ . Across the time of analysis, 57 analyses of the JND-i standard(Tanaka et  
106 al., 2000) gave a mean value of  $0.512102 \pm 0.000009$  (10.4 ppm, 1-sigma). All  $^{143}\text{Nd}/^{144}\text{Nd}$   
107 values were normalized to a preferred value of 0.512115 for JND-i. 17 analyses of standard  
108 La Jolla (Lugmair and Carlson, 1978) gave  $0.511860 \pm 0.000008$  (12.8 ppm, 1-sigma). 176  
109 analyses of NBS987 across the time of analysis gave a value of  $0.710251 \pm 0.000007$  (9 ppm,  
110 1-sigma). NBS987 standards analysed with the samples gave a value of  $0.710251 \pm 0.000007$   
111 (7.8 ppm, 1-sigma, n=14). This is within analytical uncertainty of the preferred value for this,  
112 so no secondary correction of the data was required.

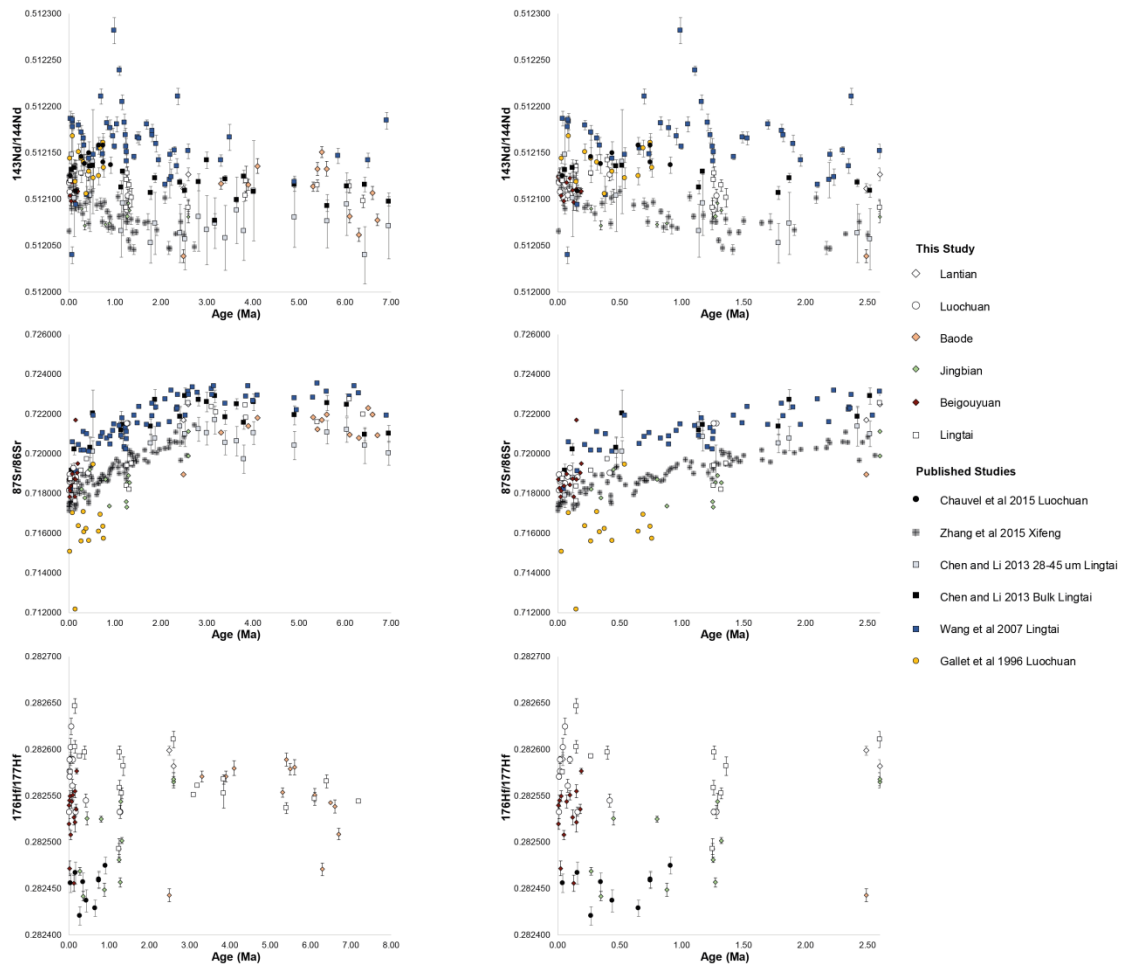
113 Hf was analysed on a Thermo-Electron Neptune mass spectrometer using a Cetac Aridus II  
114 desolvating nebuliser. 0.006 l/min of nitrogen were introduced via the nebulizer in addition  
115 to Ar in order to minimize oxide formation. The instrument was operated in static  
116 multicollection mode, with cups set to monitor  $^{172}\text{Yb}$ ,  $^{173}\text{Yb}$ ,  $^{175}\text{Lu}$ ,  $^{176}\text{Lu}+\text{Hf}+\text{Yb}$ ,  $^{177}\text{Hf}$ ,  $^{178}\text{Hf}$ ,  
117  $^{179}\text{Hf}$  and  $^{180}\text{Hf}$ . 1% dilutions of each sample were tested prior to analysis, and samples  
118 diluted to c. 20 ppb. Data are reported relative to  $^{179}\text{Hf}/^{177}\text{Hf} = 0.7325$ . The Hf standard  
119 solution JMC475 was analyzed during each analytical session and sample  $^{176}\text{Hf}/^{177}\text{Hf}$  ratios  
120 are reported relative to a value of 0.282160 for this standard. Across the 26-month period of  
121 analysis, 189 analyses of JMC475 gave a mean  $^{176}\text{Hf}/^{177}\text{Hf}$  value of  $0.282150 \pm 0.000009$  (23.1  
122 ppm, 1-sigma). Typical external precision for a single day's analysis was in the range  
123 between 13-22 ppm. Detailed results can be found in the Supplementary File.

124 Mixing hyperbolae are calculated using standard mixing equations(Faure, 2001) with  
125 average upper continental crust and bulk crust values(Rudnick and Gao, 2003) and average  
126 mantle values(Mcdonough and Sun, 1995).  $^{143}\text{Nd}/^{144}\text{Nd}$  and  $^{176}\text{Hf}/^{177}\text{Hf}$  ratios in this study are  
127 reported as  $\epsilon_{\text{Nd}}$  and  $\epsilon_{\text{Hf}}$ , using the present-day chondritic uniform reservoir (CHUR) values of  
128 0.512630 and 0.282785, respectively (Bouvier et al., 2008).

### 129 **3 RESULTS AND DISCUSSION**

#### 130 **3.1 Sr, Nd and Hf variations in within the Chinese Loess Plateau**

131 Down-section variations in Sr, Nd and Hf-isotope data for our Chinese Loess whole rock  
132 samples are shown in Fig. 2, together with published data (Chauvel et al., 2014; Chen and Li,  
133 2013; Gallet et al., 1996; Wang et al., 2007; Zhang et al., 2015). See Fig. 1 for section  
134 locations. Only published data that have been analysed using a very similar method as the  
135 samples here have been included to limit effects caused by different leaching methods.



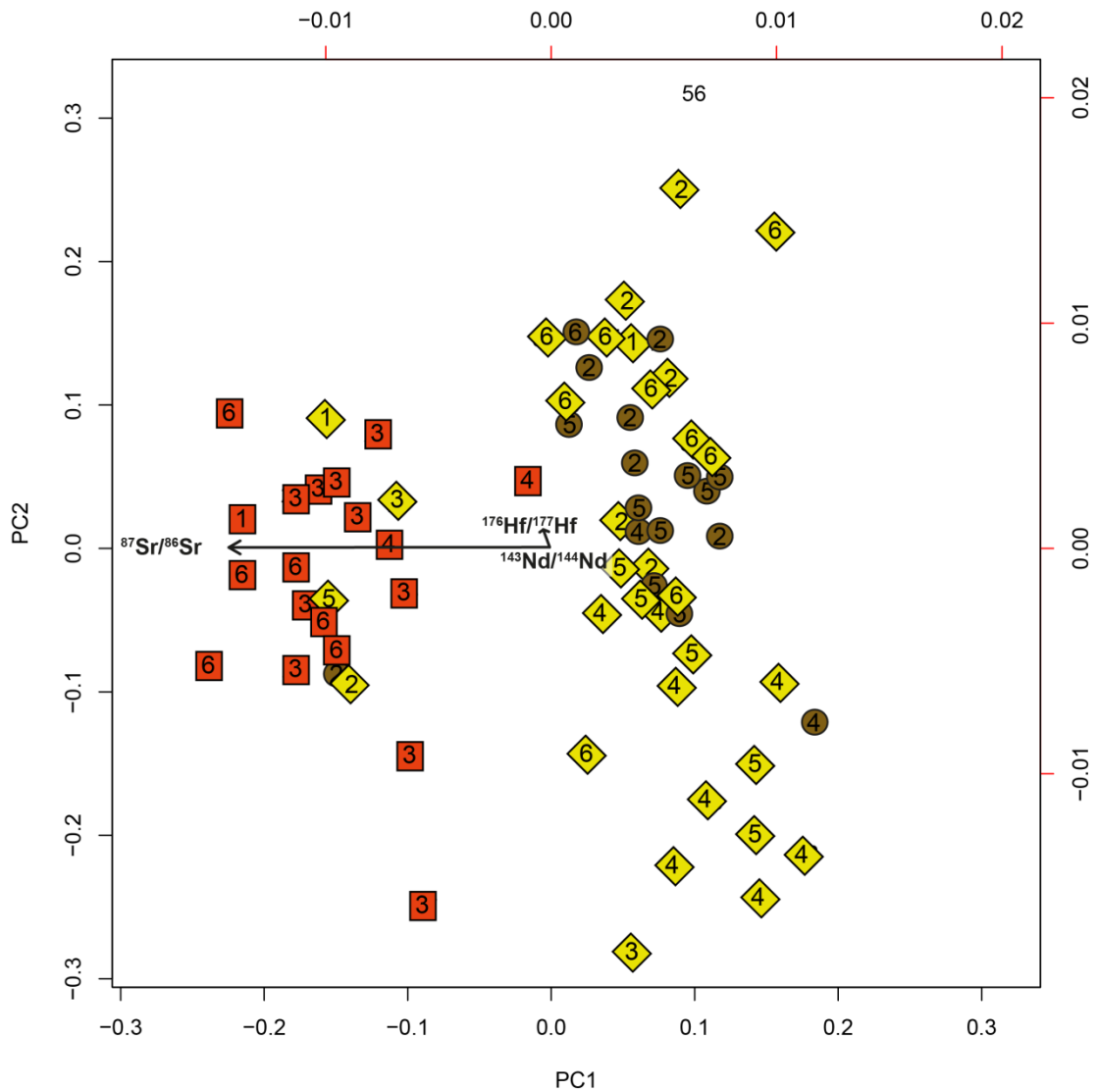
136

137 Figure 2 Isotope data from this study combined with Chauvel et al. (2015), Gallet et al. (1996), Chen and Li (2013),  
 138 Zhang et al. (2015) and Wang et al (2007) for all loess, soil and clay samples from the Chinese Loess Plateau. Data  
 139 plotted as isotopic ratios to show relative errors between datasets. Plots a, c and e show variation over 7 Ma, b, d  
 140 and f show 0 - 2.6 Ma. Age model derived from Heslop et al. 2000; Sun et al. 2006; Zhu et al. 2008; Ding et al.  
 141 1999; Wang et al. 2007; Gylesjö & Arnold 2006; Xu et al. 2009; Zhang et al. 2015.

142 Fig. 2 a) and b) show  $^{143}\text{Nd}/^{144}\text{Nd}$  plotted against the age of sediment. There is a range in the  
 143  $^{143}\text{Nd}/^{144}\text{Nd}$  values obtained from within the same units, especially from material younger  
 144 than 1 Ma. This is probably partly due to a sampling bias in that more studies have analysed  
 145 loess and soil units younger than 1 Ma. The study by Zhang et al. (2015) is the only data here  
 146 that may show a systematic decrease in  $^{143}\text{Nd}/^{144}\text{Nd}$  down-section until ~2.6 Ma where the  
 147 study stops. None of the other studies show any convincing systematic trend, nor does the  
 148 data within this study.  $^{176}\text{Hf}/^{177}\text{Hf}$  (Fig. 2 c and d) shows a similar lack of any systematic trend  
 149 down section, although this dataset suffers from the opposite problem when compared to  
 150 the Nd isotopic data in that there is much less data.  $^{87}\text{Sr}/^{86}\text{Sr}$  shows an increase until 4 Ma  
 151 where it plateaus and shows a slight decrease at 6 Ma (Fig. 2e and f). None of the isotopic  
 152 systems show an abrupt change at either 1.2 or 2.5 Ma.

153  $^{87}\text{Sr}/^{86}\text{Sr}$  is the only isotopic system to show a systematic trend related to the age of the  
 154 sediment, and there does not seem to be any correlation between  $^{87}\text{Sr}/^{86}\text{Sr}$  and the other

155 two isotopic systems, this is shown in Fig. 3 which is a PCA for all three isotopic systems. This  
 156 clearly demonstrates that there is a separate control on  $^{87}\text{Sr}/^{86}\text{Sr}$  when compared to  
 157  $^{176}\text{Hf}/^{177}\text{Hf}$  and  $^{143}\text{Nd}/^{144}\text{Nd}$ .



158 ◆ Loess ● Soil ■ Clay **1** Lantian **2** Luochuan **3** Baode **4** Jingbian **5** Beigouyuan **6** Lingtai

159 *Figure 3 PCA plot for the isotopic data from the samples within this study.*

160 As  $^{87}\text{Sr}/^{86}\text{Sr}$  is the only isotopic system showing any systematic trend it is worth exploring  
 161 what else, apart from provenance change can affect this system.  $^{87}\text{Sr}/^{86}\text{Sr}$  can be affected by  
 162 the addition of authigenic precipitates (such as carbonates). Our samples were leached in  
 163 acetic acid in order to eliminate any such effect.  $^{87}\text{Sr}/^{86}\text{Sr}$  can also be affected by chemical  
 164 weathering or enrichment of minerals rich in radiogenic  $^{87}\text{Sr}$  in fine grain-size fractions. The  
 165 highest values of  $^{87}\text{Sr}/^{86}\text{Sr}$  in our dataset are shown by the Red Clay, deposited prior to 2.5  
 166 Ma. Chemical weathering influences the  $^{87}\text{Sr}/^{86}\text{Sr}$  signal as Sr is hosted within minerals that  
 167 are readily weathered, for example, feldspar (Blum et al., 1993; White et al., 1999) and

168 easily enters solution during weathering, so is readily removed from the original sediment  
169 (Blum and Erel, 1997). This suggests that in wet/humid climates, where there is greater  
170 chemical weathering, the dissolution of feldspar leads to Sr loss resulting in concentration of  
171 relatively high Rb/Sr, high  $^{87}\text{Sr}/^{86}\text{Sr}$  minerals. This weathering effect could also explain a  
172 change in Pb isotope signatures at 2.56 Ma (Sun and Zhu, 2010), which might result from  
173 dissolution of Pb-rich minerals like apatite and allanite (Erel et al., 2004), rather than a  
174 change in source. The impact of chemical weathering on sediment composition is supported  
175 by variations in Zr/Rb ratios (Chen et al., 2006). It is also supported by evidence of shifts in  
176 the heavy mineral composition to more stable, weathering-resistant species with increasing  
177 depth in loess sections. This change has been interpreted to be due to these older units  
178 having been subjected to more humid conditions, under which less resilient minerals have  
179 undergone preferential dissolution (Bird et al., 2015; Nie, 2016; Peng et al., 2016).

180 Changes in  $^{87}\text{Sr}/^{86}\text{Sr}$  can also be driven by grain-size, where finer grain-sizes will have higher  
181  $^{87}\text{Sr}/^{86}\text{Sr}$ . At the Red Clay/loess boundary there is a change in grain-size from the finer  
182 grained Red Clay to coarser loess/soil units (Lu et al. 2010; Ding et al. 1998; Ding et al. 1999;  
183 and Yang & Ding 2010). However, both grain-sizes analysed by Chen and Li (2013) show an  
184 increasing  $^{87}\text{Sr}/^{86}\text{Sr}$  with increasing age demonstrating grain-size is not the only control on  
185  $^{87}\text{Sr}/^{86}\text{Sr}$ .

186 Rare earth elements and high field strength elements are relatively immobile during  
187 weathering; hence  $^{143}\text{Nd}/^{144}\text{Nd}$  and  $^{176}\text{Hf}/^{177}\text{Hf}$  appear to retain the character of the source  
188 material (Jung et al., 2004). These isotope systems do not systematically change at 1.2 Ma or  
189 across the Pliocene-Pleistocene boundary (Fig. 2).

190 Sr, Nd and Hf isotope data, show no evidence for major provenance changes at 2.5 or 1.2  
191 Ma. A change in provenance signal cannot therefore be used to explain the different  
192 characteristics of the loess/soil and the Red Clay units (Figs 2 & 3). The results here suggest  
193 that the change from Red Clay to loess/soil was likely to be driven by a change to a less  
194 humid climate and/or higher dust deposition rates on the CLP over the Plio-Pleistocene  
195 boundary. The constancy of dust source (at least finer grained dust) implies that there were  
196 no major changes in the origin and composition of atmospheric mineral dust over this part  
197 of Asia across a major climatic boundary. However, higher dust accumulation rates at the  
198 end of the Pliocene and into the Quaternary (Sun et al., 2011) suggest that the volume of  
199 dust material produced still increased dramatically. Combined, this implies that the volume  
200 of material produced from existing sources became greatly enhanced at the onset of the  
201 Quaternary, potentially due to a more arid climate or the integration of the Yellow River

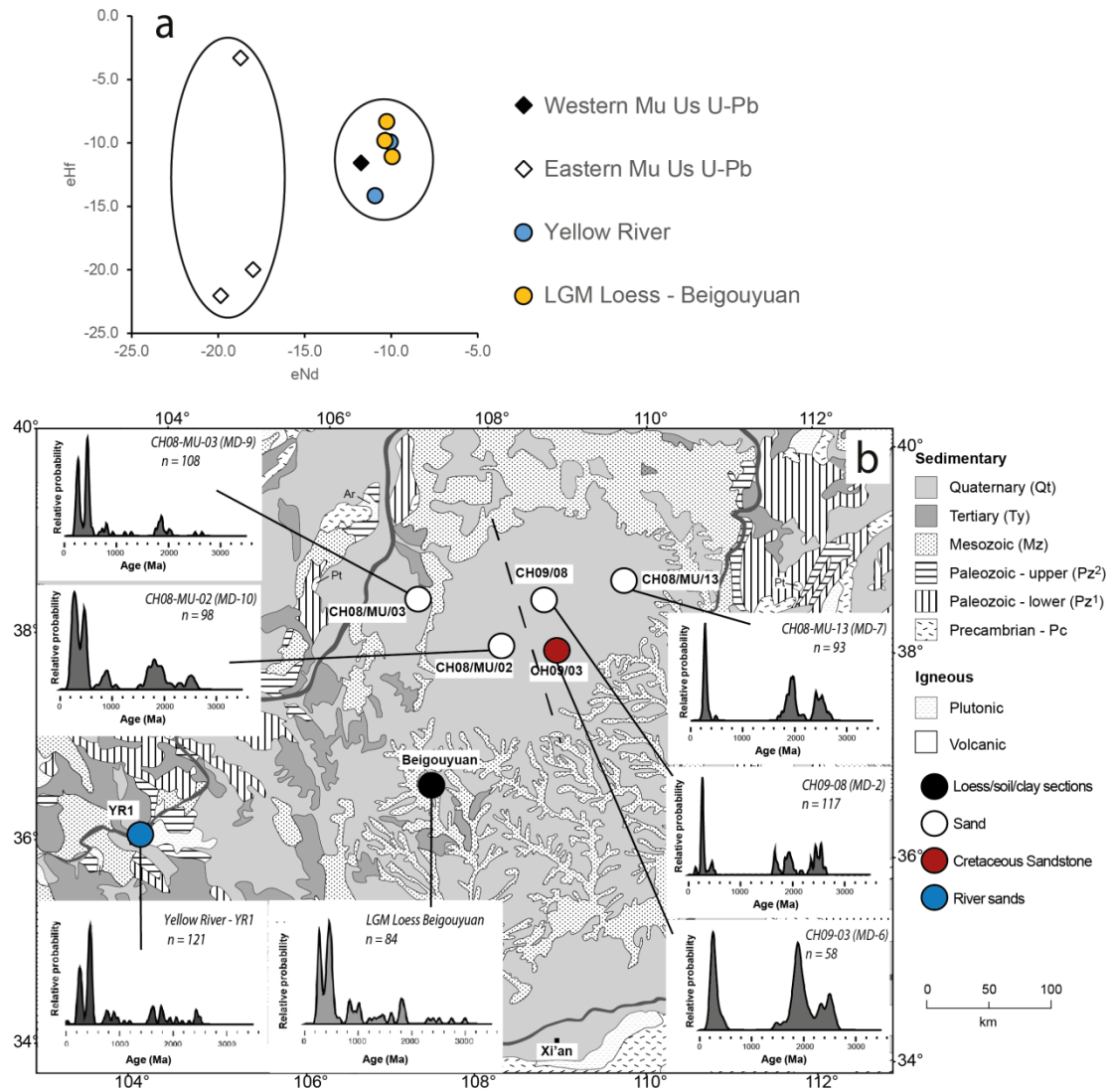
202 system, rather than there being additional supply from major new dust sources. Given that  
203 the grain size of dust sediments greatly increases at this boundary, this implies a great  
204 strengthening of dust transporting winds from these constant source areas, or also further  
205 supports the idea that a new sediment transport route occurred at the time. The Yellow  
206 River is the prime candidate for such a transport route, facilitating the transportation of  
207 coarser material from the NTP to close to the CLP where the material can then be  
208 transported through aeolian processes onto the CLP (Nie et al., 2015). However, the timing  
209 of formation of the upper Yellow River is controversial and it is also possible some reworking  
210 of coarse grained western CLP material may have also occurred (Kapp et al., 2015).

### 211 **3.2 Loess source regions**

212 Critics of bulk sediment analysis suggest it likely averages source information from the  
213 potentially multiple sediment sources to loess, thus making it difficult to identify the  
214 individual source signals. The benefit of using this method is that it considers all grain sized  
215 fractions and likely reflects signatures in the dominant source areas, and is a strong tool  
216 when used alongside with other provenance methods. Here we propose that the sensitivity  
217 of bulk sediment analyses to source differences can be tested through comparison of results  
218 to a study that identifies unambiguous sediment source differences using single-grain  
219 analyses.

220 Stevens et al. (2010; 2013) undertook provenance analysis of sediments from the Mu Us  
221 desert (Fig. 1) using zircon U-Pb and heavy mineral analysis, and showed that a clear  
222 difference in sediment source exists between the western and eastern parts of the desert. In  
223 order to test if bulk sediment isotopic analyses could detect this difference, a number of  
224 samples studied by Stevens et al. (2013) were selected for analysis. These included samples  
225 from the Mu Us Desert, the Yellow River at Zhongning, and the loess L1 (last glacial stage)  
226 from Beiguoyuan (sampled at the same depth in both studies).

227 Samples from the eastern Mu Us Desert have  $\epsilon_{Nd}$  of c. -19 and  $\epsilon_{Hf}$  of -21 whereas samples  
228 from the western part of the desert have  $\epsilon_{Nd}$  of c. -12 and  $\epsilon_{Hf}$  of -11 (Fig. 4). Notably, the  
229 samples from the western Mu Us desert have a similar signature to samples from the Yellow  
230 River, and loess from Beiguoyuan. This distinction between eastern and western Mu Us  
231 Desert signals is consistent with the conclusions of Stevens et al. (2013) using single grain  
232 methods, showing that bulk sediment isotopes will provide useful information on sediment  
233 source.



234

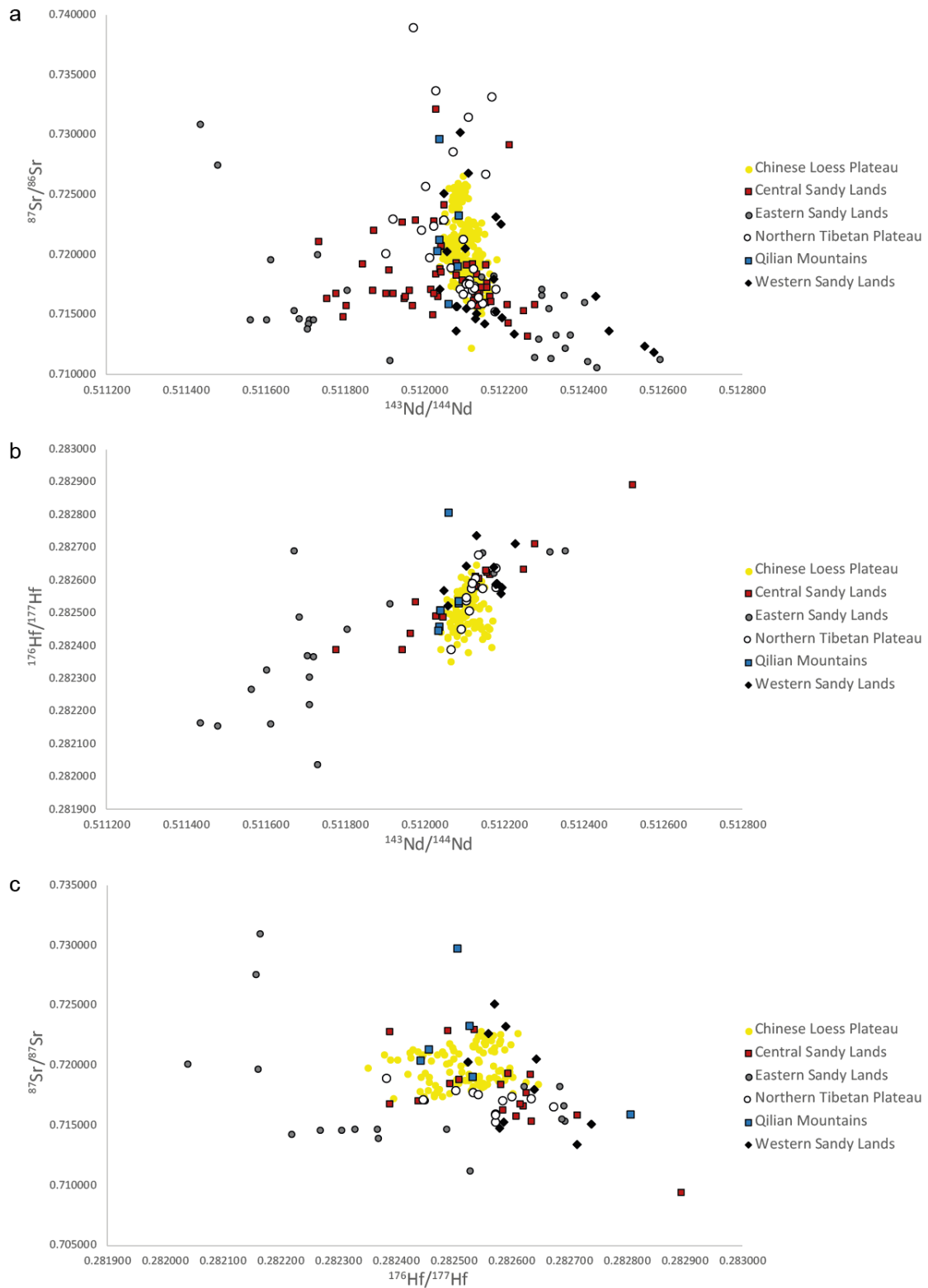
235 Figure 4  $\epsilon_{Hf}$  versus  $\epsilon_{Nd}$  for some of the Mu Us Desert samples analyzed by Stevens et al. (2013) plotted with  
 236 samples for the Yellow River, downstream of YR1 (Stevens et al., 2013) and Beigouyuan LGM (L1) loess, (b) shows  
 237 the zircon U-Pb data for these samples and their location. The dashed line is the east-west divide proposed by  
 238 Stevens et al. (2013).

239 The data reported here and the published work (Chauvel et al., 2014; Che and Li, 2013; Chen  
 240 et al., 2007; Gallet et al., 1996; Li et al., 2011; Sun, 2005; Wang et al., 2007; Zhang et al.,  
 241 2012, 2015) cover a large geographical area (Fig. 1). So to help with interpretation the data  
 242 were split into regional source areas as suggested by Licht et al. (2016); in addition, the Mu  
 243 Us Desert has been split into eastern and western regions based on Stevens et al. (2013),  
 244 Zhang et al. (2016) and the data in Fig. 4. Since the isotopic bulk sediment data includes the  
 245 very fine-grained fraction, the Tarim and Junggar basins were also added as potential  
 246 regional source areas. The regional source areas are as follows:

- 247 1. Central Sand Lands - including the Badain Jaran, Tengger, western Mu Us and Ulan  
 248 Buh deserts, and bedrock samples.

- 249 2. Eastern Sandy Lands - including Otindag and Horquin sandy lands and the eastern  
250 Mu Us desert, underlying bedrock and middle reach Yellow River samples (Nie et al.,  
251 2015).
- 252 3. Western Mu Us Desert - western China Basins (Tarim and Junggar basins).
- 253 4. Northern Tibetan Plateau - Upper Yellow River samples using the definition of upper  
254 river from Nie et al. (2015).
- 255 5. Qilian Mountains - samples from alluvial fans of rivers derived from the Qilian  
256 Mountains.

257 Nd, Hf or Sr concentrations are not often available with published isotopic data. As such,  
258 calculating potential end members of the source areas which contribute most to the Chinese  
259 Loess Plateau is impossible. Despite this several key observations and interpretations can be  
260 made from the data. Fig. 5 shows all of the data plotted up in isotopic space, the most data  
261 is on Fig. 5a which is  $^{143}\text{Nd}/^{144}\text{Nd}$  against  $^{87}\text{Sr}/^{86}\text{Sr}$ . The loess, soil and Red Clay plot in a well-  
262 defined area that is overlapped most significantly by samples from the Northern Tibetan  
263 Plateau and the Qilian Mountains with some overlap from samples from the Central and  
264 Western Sandy Lands. The Eastern Sandy Lands plot reasonably well away from the CLP  
265 samples. This is seen more clearly on Fig. 5b and Fig. 5c, indicating the dominance of more  
266 westerly or north-westerly sources.



267

268 Figure 5 Isotopic data for the Chinese Loess Plateau and the potential source areas from this study and from  
 269 Chauvel et al., (2014); Che and Li, (2013); Chen et al., (2007); Gallet et al., (1996); Li et al., (2011); Sun, (2005);  
 270 Wang et al., (2007); Zhang et al., (2012, 2015). Fig. 5a shows  $^{143}\text{Nd}/^{144}\text{Nd}$  against  $^{87}\text{Sr}/^{86}\text{Sr}$ , 5b shows  $^{143}\text{Nd}/^{144}\text{Nd}$   
 271 against  $^{176}\text{Hf}/^{177}\text{Hf}$  and 5c shows  $^{176}\text{Hf}/^{177}\text{Hf}$  against  $^{87}\text{Sr}/^{86}\text{Sr}$ .

272 All three isotopic systems show that the loess, soil and clay data overlap with the samples

273 from the Yellow River/Tibetan Plateau suggesting a Northern Tibetan Plateau source (Fig. 5a,

274 b & c). This is supported by recent hypotheses concerning sediment routing from the NTP via  
275 the Yellow River and other rivers to the CLP using single grain analysis (Bird et al., 2015; Licht  
276 et al., 2016; Nie et al., 2015, 2014; Stevens et al., 2013). There is some overlap with samples  
277 from CSL, QM and WSL with the samples from the CLP that suggest that sediment from  
278 these potential source areas are also sourced from the NTP (e.g. Chen et al., 2007; Rittner et  
279 al., 2016).

280 Previous work suggests that due to a weak NW-SE grain-size gradient in the Red Clay, in  
281 contrast to that shown in the Quaternary loess, the East Asian winter monsoon played a  
282 relatively smaller role in Red Clay deposition than in Quaternary loess deposition (Han et al.,  
283 2007; Wen, 2005). This implies that high altitude westerly winds were the main transport  
284 mechanism for dust at this time (Ding et al., 1998, 1999; Gylesjö and Arnold, 2006) and  
285 perhaps implies a change in source. A recent zircon U-Pb study also suggests a subtle source  
286 change across this boundary (Nie et al., 2015). However, heavy mineral data from Peng et al.  
287 (2016) and the lack of sediment source change shown here (Fig. 2) does not indicate a  
288 source change at the Plio-Pleistocene boundary. This means that either that the East Asian  
289 winter monsoon must also have been the main transport mechanism for the Red Clay (Peng  
290 et al., 2016), or that the westerlies transported material in the Pliocene from the same  
291 source, or a source with indistinguishable characteristics, such as that blown in by winter  
292 monsoon winds. This would be compatible with the evidence for a dominant NTP source for  
293 much of the CLP dust material (Fig. 5). An alternative explanation is that because the fine-  
294 grained fraction dominates the isotope signal, the source of this fine fraction could remain  
295 the same in loess, soil and Red Clay. By contrast, the coarse fraction may still vary due to  
296 abrupt climate shifts and changes in large dust storm tracks. This focus on different grain  
297 sizes with different provenance techniques might also explain why there is no clear variation  
298 in coarse (>10 µm) detrital zircon U-Pb age between loess and palaeosol layers (Pullen et al.,  
299 2011), although this should be seen in the Hf-Nd-Sr data. If this was the case, we might  
300 expect to see variation in Hf concentration between the Red Clay and loess relating to the  
301 proportion of zircons in the coarse fraction. However, this change is not apparent in the  
302 sample set here. In addition to this, recent grain size and zircon U-Pb work suggest that  
303 there is a SW to NE source variation within the Red Clay (Shang et al., 2016), which suggests  
304 that perhaps the East Asian Winter Monsoon played an important role in the deposition of  
305 the Red Clay as well as the Quaternary loess (Liu, 1985; An et al., 1991, Lu et al., 2000).

306 Our results support assertions that the NTP is the major dust source to the CLP over the  
307 whole Plio-Quaternary. As such, climate changes driving dust production efficiency in this

308 region are likely the main control on shifts in the dust cycle over this interval, rather than the  
309 addition of new sources by a progressive aridification over an increasing geographical area.

#### 310 **4 CONCLUSIONS**

311 The data here show that there is no source change in dust supply to the Chinese Loess  
312 Plateau at 1.2 Ma or at 2.5 Ma. Changes seen in  $^{87}\text{Sr}/^{86}\text{Sr}$  are recording grain-size and/or  
313 chemical weathering effects. The change from Red Clay to loess is likely driven by decreased  
314 humidity and increased dust deposition across the Pliocene/Quaternary transition. This  
315 study has clear implications for understanding the effects of weathering on Sr isotopes and  
316 the importance of using different provenance tools in conjunction to fully understand  
317 sediment source.

318 The isotope data shows that dust sources for the Chinese Loess Plateau are dominated by  
319 material from the Northern Tibetan Plateau. This lack of source change across the Pliocene-  
320 Pleistocene boundary suggests that the East Asian Monsoon played an important role in the  
321 deposition of the Red Clay as well as in the Quaternary loess and that the main dust  
322 transporting winds have not drastically changed trajectory since the Miocene, even if the  
323 volume of material has increased dramatically.

324 **Acknowledgements:** We thank Zhiwei Xu, Hanzhi Zhang, Lin Zeng, Han Feng for help in  
325 sampling. This research is partly granted by NERC Standard Grant (NE/I008837/1) and  
326 National Natural Science Foundation of China grants (41690111, 41472138).

327 **Author Contribution Statement:** AB, TS, MR and HL collected the samples. AB, IM and TR  
328 undertook all of the laboratory work. AB, TS, IL, PV and HL contributed to data analysis and  
329 manuscript production.

330 **Competing financial interests:** The authors declare no competing financial interests.

#### 331 **REFERENCES**

- 332 An, Z.S., Liu, T.S., Lou, Y.C., Porter, S.C., Kukla, G., Wu, X.H., Hua, Y.M., (1990). The long-term  
333 paleomonsoon variation recorded by the loess-palaeosol sequence in central China.  
334 *Quaternary International*, 7-8, 91-95.
- 335 Bird, A., Stevens, T., Rittner, M., Vermeesch, P., Carter, A., Andò, S., Garzanti, E., Lu, H., Nie,  
336 J., Zeng, L., Zhang, H., Xu, Z., 2015. Quaternary dust source variation across the Chinese  
337 Loess Plateau. *Palaeogeogr. Palaeoclimatol. Palaeoecol.* 435, 254-264.  
338 doi:10.1016/j.palaeo.2015.06.024
- 339 Blum, J.D., Erel, Y., 1997. Rb-Sr isotope systematics of a granitic soil chronosequence : The  
340 importance of biotite weathering 61, 3193-3204.
- 341 Blum, J.D., Erel, Y., Brown, K., 1993.  $^{87}\text{Sr}/^{86}\text{Sr}$  ratios of Sierra Nevada stream waters:  
342 Implications for relative mineral weathering rates. *Geochim. Cosmochim. Acta* 57,

343 5019–5025. doi:10.1016/S0016-7037(05)80014-6

344 Bouvier, A., Vervoort, J.D., Patchett, P.J., 2008. The Lu–Hf and Sm–Nd isotopic composition  
345 of CHUR: Constraints from unequilibrated chondrites and implications for the bulk  
346 composition of terrestrial planets. *Earth Planet. Sci. Lett.* 273, 48–57.  
347 doi:10.1016/j.epsl.2008.06.010

348 Chauvel, C., Garçon, M., Bureau, S., Besnault, A., Jahn, B.M., Ding, Z., 2014. Constraints from  
349 loess on the Hf–Nd isotopic composition of the upper continental crust. *Earth Planet.*  
350 *Sci. Lett.* 388, 48–58. doi:10.1016/j.epsl.2013.11.045

351 Che, X., Li, G., 2013. Binary sources of loess on the Chinese Loess Plateau revealed by U–Pb  
352 ages of zircon. *Quat. Res.* 80, 545–551. doi:10.1016/j.yqres.2013.05.007

353 Chen, J., Chen, Y., Liu, L., Ji, J., Balsam, W., Sun, Y., Lu, H., 2006. Zr/Rb ratio in the Chinese  
354 loess sequences and its implication for changes in the East Asian winter monsoon  
355 strength. *Geochim. Cosmochim. Acta* 70, 1471–1482. doi:10.1016/j.gca.2005.11.029

356 Chen, J., Li, G., Yang, J., Rao, W., Lu, H., Balsam, W., Sun, Y., Ji, J., 2007. Nd and Sr isotopic  
357 characteristics of Chinese deserts: Implications for the provenances of Asian dust.  
358 *Geochim. Cosmochim. Acta* 71, 3904–3914. doi:10.1016/j.gca.2007.04.033

359 Chen, Z., Li, G., 2013. Evolving sources of eolian detritus on the Chinese Loess Plateau since  
360 early Miocene: Tectonic and climatic controls. *Earth Planet. Sci. Lett.* 371–372, 220–  
361 225. doi:10.1016/j.epsl.2013.03.044

362 Ding, Z., Sun, J., Liu, T., Zhu, R., Yang, S., Guo, B., 1998. Wind-blown origin of the Pliocene red  
363 clay formation in the central Loess Plateau, China. *Earth Planet. Sci. Lett.* 161, 135–143.  
364 doi:10.1016/S0012-821X(98)00145-9

365 Ding, Z., Derbyshire, E., Yang, S.L., Yu, Z.W., Xiong, S.F., Liu, T.S., 2002. Stacked 2.6-Ma grain  
366 size record from the Chinese loess based on five sections and correlation with the  
367 deep-sea  $\delta^{18}\text{O}$  record. *Paleoceanography* 17, 1033. doi:10.1029/2001pa000725

368 Ding, Z.L., Rutter, N.W., Sun, J.M., Yang, S.L., Liu, T.S., 2000. Re-arrangement of atmospheric  
369 circulation at about 2.6 Ma over northern China: Evidence from grain size records of  
370 loess-palaeosol and red clay sequences. *Quat. Sci. Rev.* 19, 547–558.  
371 doi:10.1016/S0277-3791(99)00017-7

372 Ding, Z.L., Xiong, S.F., Sun, J.M., Yang, S.L., Gu, Z.Y., Liu, T.S., 1999. Pedostratigraphy and  
373 paleomagnetism of a  $\approx 7.0$  Ma eolian loess – red clay sequence at Lingtai, Loess  
374 Plateau, north-central China and the implications for paleomonsoon evolution 152,  
375 49–66.

376 Erel, Y., Blum, J.D., Roueff, E., Ganor, J., 2004. Lead and strontium isotopes as monitors of  
377 experimental granitoid mineral dissolution. *Geochim. Cosmochim. Acta* 68, 4649–4663.  
378 doi:10.1016/j.gca.2004.04.022

379 Faure, G., 2001. *Origin of Igneous Rocks*. doi:10.1007/978-3-662-04474-2

380 Gallet, S., Jahn, B., Torii, M., 1996. Geochemical characterization of the Luochuan loess-  
381 paleosol sequence, China, and paleoclimatic implications 2541.

382 Guo, Z.T., Ruddiman, W.F., Hao, Q.Z., Wu, H.B., Qiao, Y.S., 2002. Onset of Asian deserti-  
383 cation by 22 Myr ago inferred from loess deposits in China 159–163.

384 Gylesjö, S., Arnold, E., 2006. Clay mineralogy of a red clay–loess sequence from Lingtai, the  
385 Chinese Loess Plateau. *Glob. Planet. Change* 51, 181–194.  
386 doi:10.1016/j.gloplacha.2006.03.002

387 Han, J., Chen, H., Fyfe, W.S., Guo, Z., Wang, D., Liu, T.S., 2007. Spatial and temporal patterns  
388 of grain size and chemical weathering of the Chinese Red Clay Formation and

389 implications for East Asian monsoon evolution. *Geochim. Cosmochim. Acta* 71, 3990–  
390 4004. doi:10.1016/j.gca.2007.05.027

391 Heslop, D., Langereis, C.G., Dekkers, M.J., 2000. A new astronomical timescale for the loess  
392 deposits of Northern China. *Earth Planet. Sci. Lett.* 184, 125–139. doi:10.1016/S0012-  
393 821X(00)00324-1

394 Jahn, B., Gallet, S., Han, J., 2001. Geochemistry of the Xining, Xifeng and Jixian sections,  
395 Loess Plateau of China: eolian dust provenance and paleosol evolution during the last  
396 140 ka.

397 Jung, S.J. a., Davies, G.R., Ganssen, G.M., Kroon, D., 2004. Stepwise Holocene aridification in  
398 NE Africa deduced from dust-borne radiogenic isotope records. *Earth Planet. Sci. Lett.*  
399 221, 27–37. doi:10.1016/S0012-821X(04)00095-0

400 Li, G., Pettke, T., Chen, J., 2011. Increasing Nd isotopic ratio of Asian dust indicates  
401 progressive uplift of the north Tibetan Plateau since the middle Miocene. *Geology* 39,  
402 199–202. doi:10.1130/G31734.1

403 Licht, A., Pullen, A., Kapp, P., Abell, J., Giesler, N., 2016. Eolian cannibalism: Reworked loess  
404 and fluvial sediment as the main sources of the Chinese Loess Plateau. *Geol. Soc. Am.*  
405 *Bull.* 128, 944–956. doi:10.1130/B31375.1

406 Liu, T.S., (1985). In: *Loess and Environment*. China Ocean Press, Beijing, pp. 149–226.

407 Lu, H. Y., & Sun, D. H. (2000). Pathways of dust input to the Chinese Loess Plateau during the  
408 last glacial and interglacial periods. *Catena*, 40, 251–261.

409 Lu, H., 2015. Driving force behind global cooling in the Cenozoic: an ongoing mystery. *Sci.*  
410 *Bull.* 60, 2091–2095. doi:10.1007/s11434-015-0973-y

411 Lu, H., Wang, X., Li, L., 2010. Aeolian sediment evidence that global cooling has driven late  
412 Cenozoic stepwise aridification in central Asia. *Geol. Soc. London, Spec. Publ.* 342, 29–  
413 44. doi:10.1144/SP342.4

414 Lugmair, G.W., Carlson, R.W., 1978. The Sm-Nd history of KREEP. *Proc. Lunar Planet. Sci.*  
415 *Conf.* 9, 689–704.

416 McDonough, W.F., Sun, S.-., 1995. McDonough & Sun 1995 Chondrite PM Comp.pdf. *Chem.*  
417 *Geol.* 120, 223–253.

418 Merkel, U., Rousseau, D., Stuut, J., Winckler, G., Gunten, L. Von, Kiefer, T., 2014. Past Global  
419 Changed Magazine, vol. 22(2), 57–116.

420 Nie, J., Peng, W., Möller, A., Song, Y., Stockli, D.F., Stevens, T., Horton, B.K., Liu, S., Bird, A.,  
421 Oalman, J., Gong, H., Fang, X., 2014. Provenance of the upper Miocene–Pliocene Red  
422 Clay deposits of the Chinese loess plateau. *Earth Planet. Sci. Lett.* 407, 35–47.  
423 doi:10.1016/j.epsl.2014.09.026

424 Nie, J., Stevens, T., Rittner, M., Stockli, D., Garzanti, E., Limonta, M., Bird, A., Andò, S.,  
425 Vermeesch, P., Saylor, J., Lu, H., Breecker, D., Hu, X., Liu, S., Resentini, A., Vezzoli, G.,  
426 Peng, W., Carter, A., Ji, S., Pan, B., 2015. Loess Plateau storage of Northeastern Tibetan  
427 Plateau-derived Yellow River sediment. *Nat. Commun.* 6, 8511.  
428 doi:10.1038/ncomms9511

429 Peng, W., Wang, Z., Song, Y., Pfaff, K., Luo, Z., Nie, J., Chen, W., 2016. A comparison of heavy  
430 mineral assemblage between the loess and the Red Clay sequences on the Chinese  
431 Loess Plateau. *Aeolian Res.* 21, 87–91. doi:10.1016/j.aeolia.2016.02.004

432 Porter, S.C., Hallet, B., Wu, X., An, Z., 2001. Dependence of Near-Surface Magnetic  
433 Susceptibility on Dust Accumulation Rate and Precipitation on the Chinese Loess

434 Plateau. *Quat. Res.* 55, 271–283. doi:10.1006/qres.2001.2224

435 Pullen, A., Kapp, P., McCallister, A.T., Chang, H., Gehrels, G.E., Garzione, C.N., Heermance, R.  
436 V., Ding, L. 2011. Qaidam Basin and northern Tibetan Plateau as dust sources for the  
437 Chinese Loess Plateau and paleoclimatic implications. *Geology* 39, 1031–1034.  
438 doi:10.1130/G32296.1

439 Rudnick, R., Gao, S., 2003. Composition of the Continental Crust. *Treatise on Geochemistry*,  
440 Vol. 3, 1-64.

441 Shang, Y., Beets, C.J., Tang, H., Prins, M.A., Lahaye, Y., van Elsas, R., Sukselainen, L.,  
442 Kaakinen, A., 2016. Variations in the provenance of the late Neogene Red Clay deposits  
443 in northern China. *Earth Planet. Sci. Lett.* 439, 88–100. doi:10.1016/j.epsl.2016.01.031

444 Stevens, T., Carter, a., Watson, T.P., Vermeesch, P., Andò, S., Bird, a. F., Lu, H., Garzanti, E.,  
445 Cottam, M. a., Sevastjanova, I., 2013. Genetic linkage between the Yellow River, the  
446 Mu Us desert and the Chinese Loess Plateau. *Quat. Sci. Rev.* 78, 355–368.  
447 doi:10.1016/j.quascirev.2012.11.032

448 Stevens, T., Lu, H., 2010. Radiometric dating of the late Quaternary summer monsoon on the  
449 Loess Plateau, China. *Geol. Soc. London, Spec. Publ.* 342, 87–108. doi:10.1144/SP342.8

450 Sun, D., Su, R., Li, Z., Lu, H., 2011. The ultrafine component in Chinese loess and its variation  
451 over the past 7·6 Ma: implications for the history of pedogenesis. *Sedimentology* 58,  
452 916–935. doi:10.1111/j.1365-3091.2010.01189.x

453 Sun, J., 2005. Nd and Sr isotopic variations in Chinese eolian deposits during the past 8 Ma:  
454 Implications for provenance change. *Earth Planet. Sci. Lett.* 240, 454–466.  
455 doi:10.1016/j.epsl.2005.09.019

456 Sun, J., Zhu, X., 2010. Temporal variations in Pb isotopes and trace element concentrations  
457 within Chinese eolian deposits during the past 8Ma: Implications for provenance  
458 change. *Earth Planet. Sci. Lett.* 290, 438–447. doi:10.1016/j.epsl.2010.01.001

459 Sun, Y., Lu, H., An, Z., 2006. Grain size of loess, palaeosol and Red Clay deposits on the  
460 Chinese Loess Plateau: Significance for understanding pedogenic alteration and  
461 palaeomonsoon evolution. *Palaeogeogr. Palaeoclimatol. Palaeoecol.* 241, 129–138.  
462 doi:10.1016/j.palaeo.2006.06.018

463 Sun, Y., Tada, R., Chen, J., Liu, Q., Toyoda, S., Tani, A., Ji, J., Isozaki, Y., 2008. Tracing the  
464 provenance of fine-grained dust deposited on the central Chinese Loess Plateau.  
465 *Geophys. Res. Lett.* 35, 1–5. doi:10.1029/2007GL031672

466 Tanaka, T., Togashi, S., Kamioka, H., Amakawa, H., 2000. JNdi-1: a neodymium isotopic  
467 reference in consistency with LaJolla neodymium. *Chemical Geology*, Vol. 168, 279–  
468 281.

469 Vermeesch, P., Resentini, A., Garzanti, E., 2016. An R package for statistical provenance  
470 analysis. *Sediment. Geol.* 336, 14–25. doi:10.1016/j.sedgeo.2016.01.009

471 Wang, Y.-X., Yang, J.-D., Chen, J., Zhang, K.-J., Rao, W.-B., 2007. The Sr and Nd isotopic  
472 variations of the Chinese Loess Plateau during the past 7 Ma: Implications for the East  
473 Asian winter monsoon and source areas of loess. *Palaeogeogr. Palaeoclimatol.*  
474 *Palaeoecol.* 249, 351–361. doi:10.1016/j.palaeo.2007.02.010

475 Watson, a J., Bakker, D.C., Ridgwell, a J., Boyd, P.W., Law, C.S., 2000. Effect of iron supply  
476 on Southern Ocean CO<sub>2</sub> uptake and implications for glacial atmospheric CO<sub>2</sub>. *Nature*  
477 407, 730–733. doi:10.1038/35037561

478 Wen, L., 2005. Changes in grain-size and sedimentation rate of the Neogene Red Clay  
479 deposits along the Chinese Loess Plateau and implications for the palaeowind system .